Computationally Efficient Simulation of Floating Dual-Body Point Absorber

Aengus Connolly [*], Gerard O'Mahony[*], Aonghus O'Connor[*]

[*] Digital Solutions, Wood

Abstract- This paper describes a computationally efficient numerical simulation methodology which may be used to model wave energy converters in power-production mode with high levels of accuracy. The technique combines a linear, boundary element model of the hydrodynamic forces, with a non-linear finite element simulation of the structural response. Verification of the methodology centres on a floating point absorber which was designed by the U.S. Department of Energy as part of their reference model project.

The presented simulation methodology has been implemented in a commercial product, and its validation process considers code-to-code benchmarks with other software, and comparisons with experimental data derived from model-scale tank test facilities. Several different scenarios are considered as part of the validation, beginning with simple response decay tests, before progressing to regular wave loading, and a full random seastate scatter diagram. Results of interest include floating body motions, mooring line tensions, and generated electrical power, all of which show close correlation with the reference data sources.

Numerical simulation of an entire scatter diagram in the time domain can be quite computationally expensive, so an economical extrapolation technique is also investigated with a view to estimating the entire power production matrix based on a selection of 'reference seastates' within the scatter diagram. Despite its inherent simplicity, this extrapolation approach has the potential to expedite preliminary feasibility studies, and accelerate initial screening processes which determine the overall suitability of a given wave energy converter in a particular geographical location.

Keywords- Computationally Efficient, Flexcom, Numerical Simulation, Renewable Energy, Wave Energy

I. INTRODUCTION

Detailed numerical models allow wave energy converter (WEC) developers to gain a deeper understanding of the device's behaviour. Additional insights gained from realistic engineering simulations facilitate design optimisation for improved efficiency, enable the exploration of potential advances in energy generation, and assist in the identification of opportunities for cost reduction.

WEC developers require software modelling tools to expedite the refinement and optimisation of their concepts. Simulation software typically falls into one of three main categories: products which are specifically dedicated to modelling WECs, products which specialise in marine engineering but which are not solely restricted to WECs, and completely general-purpose engineering software. In an effort to reduce entry barriers to new developers and facilitate growth of the wave energy sector in general, the U.S. Department of Energy (USDOE) commissioned the development of a free-to-use software product called 'WEC-Sim' (Wave Energy Convertor SIMulator). This has been jointly developed by the National Renewable Energy Laboratory (NREL) and Sandia National Laboratories under the auspices of a government funded initiative [1]. The software under consideration in this study is an offshore marine engineering simulator called 'Flexcom' [2]. Although traditionally used in offshore oil and gas, its capabilities have recently been extended in the area of wave energy simulation via the introduction of a dedicated module, 'Flexcom Wave'. ANSYS Aqwa is a hydrodynamic modelling package which uses radiation-diffraction theory to characterise the hydrodynamic loading on a floating body. Pressure forces can be transferred to structural mechanics products for subsequent structural analysis. The full suite of ANSYS products offers a comprehensive modelling facility and covers most fields of engineering simulation.

Ruehl et al. [3] observe that many existing commercial codes are limited in their ability to model WECs, due to their legacy focus on traditional naval architecture applications. For example, they note that WECs are often multi-body systems which have significant hydrodynamic interaction with the incident waves, and typically have complex PTO systems. While retaining its traditional modelling capabilities, recent extensions to Flexcom have also facilitated its adoption as a WEC simulator, addressing some of the limitations associated with generic commercial codes:

- Multi-body WECs are readily supported. Hydrodynamic coupling between adjacent bodies is

achieved by user-defined co-influence added mass and radiation damping matrices. In this case, the off-diagonal terms of the co-influence matrices give rise to additional terms which are incorporated into the equations of motion.

- Complex PTOs may be simulated using a combination of non-linear spring and damper elements [4].
- Structural analysis of mooring lines and mechanical linkages is performed accurately using a full finite element formulation [5, 6]. Up to 10 integration points may be included per element to ensure a precise distribution of applied forces, while second order shape functions are used to predict solution variations within each element. By comparison WEC-Sim uses a simpler structural modelling technique provided by MoorDyn, an open-source lumped-mass mooring dynamics model [7].
- The engineering simulator is compatible with a financial appraisal product called 'ExceedenceFinance', which examines commercial feasibility of renewable energy devices [8]. As well as predicting financial indicators like levelised cost of energy, this software also supplies environmental conditions from open metocean datasets.

II. REFERENCE MODEL

The Reference Model Project (RMP) was initiated by the USDOE with the aim of developing open-source designs as reference models to benchmark marine energy technology performance and costs [9]. Specific study objectives included the development of a methodology for design and economic analysis of marine energy technologies, and the application of this methodology to design and analyse open-source reference devices paired with reference marine energy resource sites. Among the six device types considered, the third reference model (RM3) was a point absorber type wave energy conversion device.

The RM3 wave energy device was designed for a reference site located offshore of Eureka in Humboldt County, California. The device concept was inspired by a device known as 'PowerBuoy' [10], which is a two-body floating point absorber design. The device consists of a surface float which moves in response to wave motion, relative to a vertical column spar buoy which is attached to a large reaction plate which is submerged at a depth of approximately 35 metres below the mean water line. Stability of the device is ensured via a spread mooring configuration, and it is designed to operate in water depths of between 40 and 100 metres. Generation of electrical power occurs predominately by harnessing oscillations of the surface float in the heave direction. The device developers anticipate that optimum energy capture occurs when the system is at resonance – i.e. when the oscillations of the floating body are in-phase with the wave excitation forces [11]. The device design is shown in Figure 1.

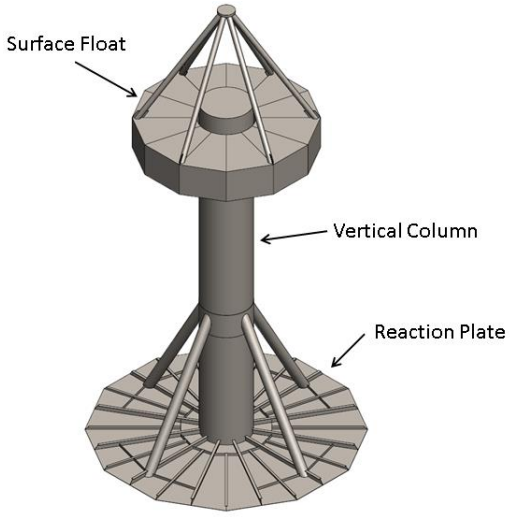

Figure 1 : RM3 device design [11]

III. COMPUTATIONAL METHODOLOGY

The velocity potential is classically decomposed into incident, diffraction and radiated potentials (Eq. 1). Incident potential represents the wave excitation, diffraction represents disturbance of the wave induced fluid motion due to the presence of a fixed body, while the radiated potential represents the fluid motion caused by a moving body in still water.

$$\Phi = \Phi_I + \Phi_D + \Phi_R \qquad (1)$$

Time domain simulation codes (such as the ones listed above) typically use an established impulse response formulation known as the Cummins integral [12] to formulate the equations of motion of a floating body in the time domain. The formulation was originally developed to allow naval architects to simulate ship motions, but it has since been adopted by the wave energy community. The fundamental equation of motion for a WEC is stated as follows:

$$[M + m(\infty)]\ddot{x} + \int_{-\infty}^{t} R(t-\tau)\dot{x}(\tau)d\tau + K_{hs}x = f_e(t) + f_m(t) + f_{PTO}(t) \qquad (2)$$

where M is the WEC mass, m(∞) is the added mass at infinite frequency, the convolution integral represents the wave radiation force, K_{hs} is the hydrostatic stiffness matrix, f_e is the wave excitation force, f_m are the external forces due to the mooring lines, and f_{PTO} is the force induced by the PTO. The x vector represents the WEC motions in six degrees of freedom (heave, surge, sway, yaw, roll and pitch), with the derivative terms corresponding to velocity and acceleration respectively. It is noteworthy that Eq.2 effectively separates the total hydrodynamic force into excitation (incident plus diffraction) and radiation

components based on the flow potential (Eq. 1). Radiation-diffraction programs such as WAMIT [13] and NEMOH [14] solve the radiation and diffraction potentials, and provide coefficient terms at a range of discrete frequencies which may be readily inserted into Eq. 2.

The approach taken in this study is effectively a hybrid of linear and non-linear modelling techniques. Hydrodynamic excitation forces on the WEC are simulated in a linear manner, based on the linear solution to potential flow theory, while the structural aspects such as mooring line dynamics and power take-off (PTO) are modelled in a fully non-linear fashion using a finite element technique. Although this is a common approach in recent times and has proven applicable to the range of sea conditions most relevant to power production, it is worth noting that linear hydrodynamics are not valid for stormy conditions when devices can undergo large excursions relative to the incident wave elevation. The linear approach to hydrodynamics is justified based on the following assumptions:

- Numerical simulations are focused on the power-production mode, hence the simulated load cases represent operating conditions. Non-linear effects become much more pronounced in severe seastates, but in such conditions the device typically switches to survival mode where power production is abandoned.
- The device under consideration has a relatively simple geometry, so the immersed cross-sectional area does not vary significantly over time (the surface float is effectively a cylinder). It has been shown that non-linear hydrodynamics are not as critical for geometries of uniform cross-sectional area [15].
- The majority of the spar remains submerged beneath the free surface at all times, so the assumption of hydrodynamic linearity on this section appears logical.

IV. SOFTWARE MODEL

The two floating bodies, both the surface float and the spar buoy, are represented by separate assemblages of rigid massless beam elements. This effectively serves as a framework upon which the various constituents may be applied. Finite element nodes are placed at locations corresponding to the centre of gravity (CoG) and centre of buoyancy (CoB) of each body. Mass and rotational inertia terms are concentrated at each CoG node, while hydrostatic stiffness terms at the CoB nodes are used to simulate the restoring forces due to changes in buoyancy as the bodies deviate from their mean positions. Wave excitation force coefficients, plus added mass and damping terms, are computed separately by NEMOH across a broad range of frequencies, and associated with the relevant CoG nodes in the structural model. The spar buoy is held on station using three mooring lines evenly spaced at 120 degrees apart. These lines are explicitly modelled using finite elements of appropriate structural properties, and attached to the spar buoy at the fairlead locations. A flat seabed is assumed for consistency with the WEC-Sim model and the test tank, although the solver also supports arbitrary seabed profiles.

The PTO is represented as a cylindrical piston-and-sleeve type device, an approach which is suitable whether the mechanism is a hydraulic or pneumatic piston, or a linear electric generator. Power extraction is modelled using a non-linear damper element. The axial force exerted by the damper element, F, is defined as follows:

$$F = -(F_0 + C_1 v) \qquad (3)$$

where v is the relative velocity between the element end nodes in the axial direction, F_0 is the constant damping force, and C_1 is the linear damping coefficient. The power produced by the damper element is calculated as follows:

$$P = -Fv \qquad (4)$$

The end stops of the PTO are modelled using a non-linear spring element. In regions of free movement, the spring offers no resistance to extension or contraction. As the PTO extends or contracts towards its maximum stroke-out, the spring stiffness is increased to provide a high level of resistance to any further motion.

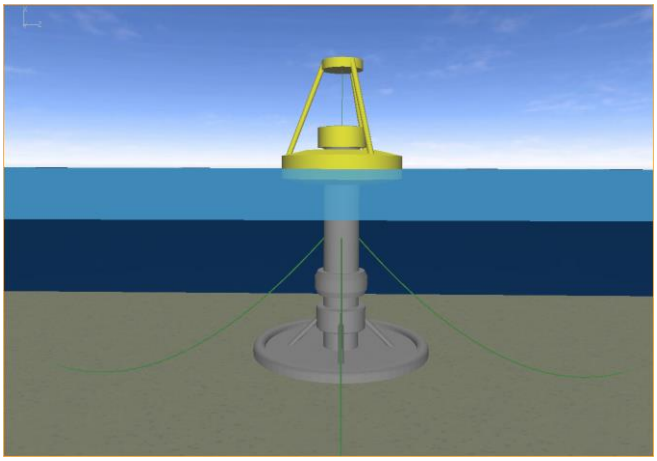

Figure 2 : Software model of RM3 device

V. REGULAR WAVE ANALYSIS

In order to ensure accuracy of the wave excitation forces in the software model, a single regular wave simulation was performed to examine the device's response in various directions. The mooring lines and PTO were omitted to focus purely on the motion characteristics of the device itself. For illustrative purposes, a sample wave of 2.5m height and 12s period was applied. In the context of the ambient conditions at the Eureka site, this would be considered to represent medium conditions in terms of both wave height and period. The inherent simplicity of a regular wave simulation means that it is possible to directly compare time histories between Flexcom and WEC-Sim.

Results in heave (float), heave (spar), surge and pitch are presented in Figure 3 to Figure 6 respectively.

Excellent agreement is obtained for the heave response of the surface float, while the heave motions of the spar also show very close agreement. Excellent agreement is also obtained for the pitch response of the device (both the float and spar buoy pitch together in unison). The surge motions predicted by Flexcom are periodic as expected, and consistent with the regular nature of the excitation. WEC-Sim also shows a periodic response, but with the device gradually drifting away. When questioned on the source of this motion, the WEC-Sim technical support team suggested that this phenomenon is caused by a small, numerically-induced force imbalance in the surge direction, related to the implementation of the ramp function and multi-DOF coupling in the software. In any case the issue is not significant as surge motions would be constrained in reality due to the mooring system, and additionally the device's power production is largely independent of surge.

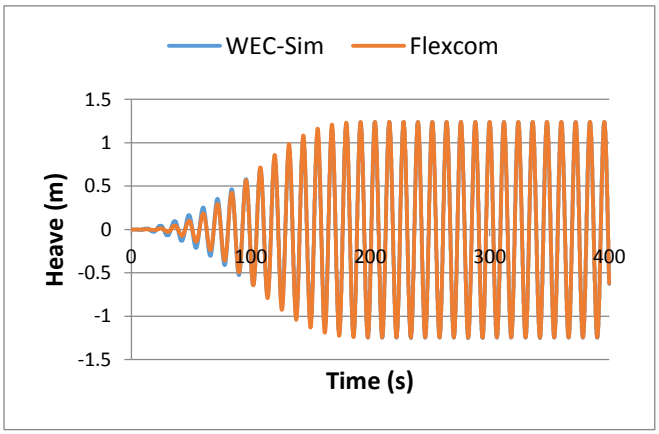

Figure 3 : Periodic Heave Response (Surface Float)

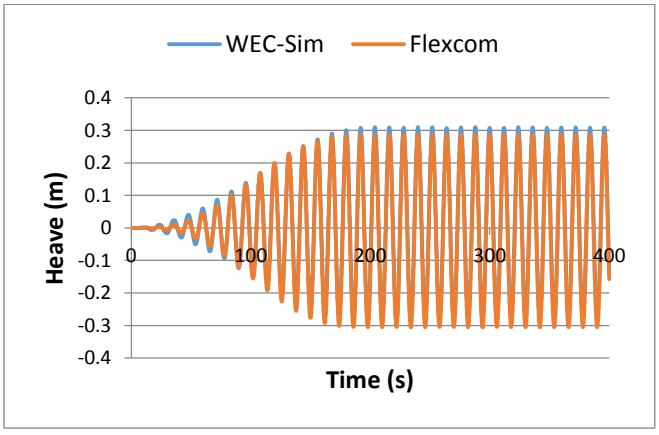

Figure 4 : Periodic Heave Response (Spar Buoy)

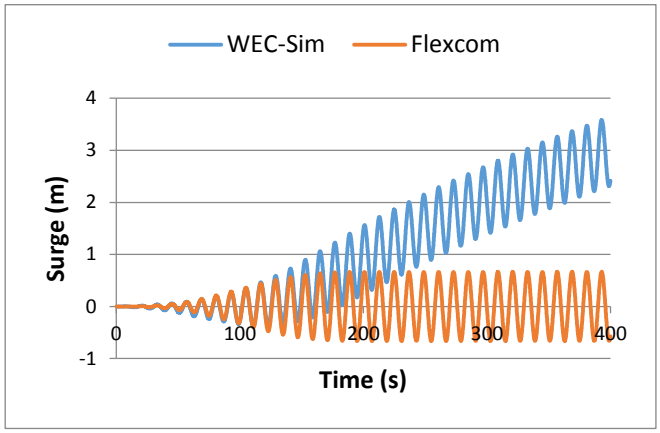

Figure 5 : Periodic Surge Response

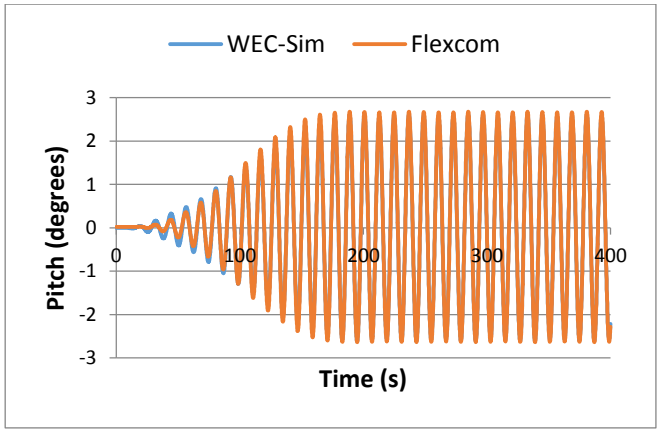

Figure 6 : Periodic Pitch Response

VI. EUREKA SITE

The wave energy resource for the RM3 device is based on available information from the Eureka site. This particular location was identified by the USDOE as it has a wave climate representative of the US's west coast, and moreover a wide range of high-fidelity oceanographic data sets is readily available for this area. Figure 7 and Figure 8 present the mechanical power matrix for the Eureka site as predicted by Flexcom, in both graphical and tabular format.

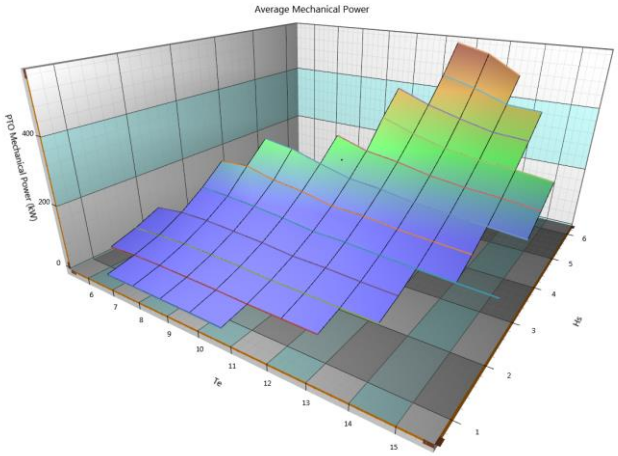

Figure 7 : Mechanical Power Plot for Eureka Site

Wave Period - Te (s)

Wave Height - Hs (m)	4.5	5.5	6.5	7.5	8.5	9.5	10.5	11.5	12.5	13.5	14.5	15.5	16.5
0.25													
0.75			10	10	10	9	8						
1.25		22	28	28	27	25	22	21	20				
1.75		46	52	56	53	50	44	42	40	38			
2.25		80	92	93	87	82	72	70	66	62			
2.75			144	139	132	122	108	106	98	93	88	84	
3.25			206	210	187	174	152	148	137	130	124		
3.75				277	262	234	208	198	182	173	166	158	
4.25						301	269	255	234	221	214	204	
4.75							355	320	293	276	268	255	
5.25							430	391	362	336	328		
5.75								468	440	402	394		
6.25								560	533	475			
6.75													

Figure 8 : Mechanical Power Matrix for Eureka Site

The full scatter diagram for the Eureka test site contains a total of 84 different seastates with non-zero percentage occurrences, spanning across 11 different periods and 12 different wave heights. For the purposes of software benchmarking, it is difficult to visually compare two sets of data in 3-dimensions. So in order to facilitate comparisons, Figure 9 presents a 2D plot of mechanical power as function of wave period. This plot compares the mechanical power predicted by the software with the official Sandia report on the RM3 device [11, p.147]. Note that the wave height varies across each period, approximately corresponding to the weighted average wave height experienced at that particular period. The seastates selected for benchmarking are highlighted by red markers in the scatter diagram presented in Figure 10.

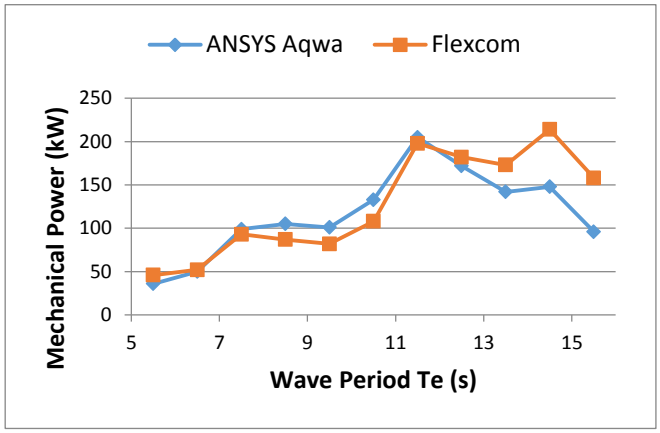

Figure 9 : Mechanical Power at Eureka Site for Selected Seastates

Wave Period - Te (s)

Wave Height - Hs (m)	4.5	5.5	6.5	7.5	8.5	9.5	10.5	11.5	12.5	13.5	14.5	15.5	16.5
0.25													
0.75			0.6	0.8	0.5	0.5	0.2						
1.25		1	2.7	3.7	4.1	2.9	1.5	0.4	0.1				
1.75		1	4.4	4.3	4.1	3.4	2	1.1	0.6	0.1			
2.25		0.2	3.5	4.2	3.6	4.1	3.1	1.5	1.2	0.3			
2.75			1.5	2.5	1.9	3.2	3.3	1.8	1.1	0.4	0.1	0.1	
3.25			0.1	0.9	0.9	2	2.4	1.4	0.8	0.4	0.1		
3.75				0.1	0.2	1	1.9	1.5	0.5	0.3	0.2	0.1	
4.25						0.2	1	1.3	0.5	0.3	0.2	0.1	
4.75							0.3	0.4	0.4	0.2	0.1	0.1	
5.25							0.1	0.2	0.3	0.2	0.1		
5.75								0.2	0.1	0.1	0.1		
6.25								0.1	0.1	0.1			
6.75													

Figure 10 : Wave Scatter Diagram showing Selected Seastates

Close agreement of power output is demonstrated between the data sources for low to medium wave periods. Some discrepancies begin to become apparent for the upper wave periods, where Flexcom appears to overestimate the mechanical power from the device. A qualitative assessment of the overall trend suggests that the results are consistent with expectations as both data sets are generally well aligned. As noted earlier, the hydrodynamic excitation forces in the numerical solver are based on a linear solution to potential flow theory. This approach assumes that displacements of the free surface and the floating body away from their mean positions remain relatively small, an assumption which becomes increasingly challenged for more severe seastates. By contrast the benchmark data was generated using a time-domain radiation and diffraction simulation in ANSYS Aqwa [16], allowing non-linear effects to be captured more accurately. Moreover this data was subsequently validated using RANS-based (Reynolds-Averaged Navier-Stokes) computational fluid dynamics (CFD) simulations [17]. Results from the CFD studies showed that non-linear hydrodynamic effects can have a significant influence on the response of the floating point absorber, particularly at larger wave heights where these effects become more pronounced. For example, the power

generation efficiency for the device in 4.0m waves is much lower than in 2.5m waves. Sources of non-linearity at large wave heights include viscous drag caused by flow separation and vortex shedding, wave overtopping forces, and slamming loads when the upper float re-enters the water surface from above.

The preceding figures focused solely on mechanical power to provide complete transparency regarding the software benchmarking exercise, as this is the most basic measure of power output). In reality the measures of primary concern to a WEC designer are (i) electrical power and (ii) annual energy production (AEP). A power conversion efficiency factor is used to account for the losses between the generated mechanical power and the actual electrical power output. Neary et al. [11] suggest that a hydraulic power conversion chain is used in the RM3 device, and assume a conversion efficiency of 80% as reported by Cargo et al. [18]. Additionally the electrical power matrix is capped at the maximum power rating of the device, which helps to limit the size and cost of the electrical generator. Figure 11 shows the predicted electrical power matrix, and it is clear that the device achieves its maximum power rating for many of the larger seastates.

Wave Height - Hs (m) \ Wave Period - Te (s)	4.5	5.5	6.5	7.5	8.5	9.5	10.5	11.5	12.5	13.5	14.5	15.5	16.5
0.25													
0.75		7	8	8	8	7	6	6	6	6	5	5	
1.25		19	21	23	22	20	18	18	16	15	15	14	
1.75		37	42	45	42	40	35	34	32	30	29	28	
2.25		61	69	74	70	65	58	57	52	50	48	46	
2.75		91	103	111	104	98	87	85	78	74	72	68	
3.25		127	144	155	146	136	121	119	109	104	100	95	
3.75		170	192	206	194	182	161	158	145	138	133	127	
4.25		218	246	265	249	233	207	203	187	178	171	163	
4.75		272	286	286	286	286	259	254	233	222	214	203	
5.25		286	286	286	286	286	286	286	285	271	261	248	
5.75		286	286	286	286	286	286	286	286	286	286	286	
6.25		286	286	286	286	286	286	286	286	286	286	286	
6.75													

Figure 11 : Electrical Power Matrix for Eureka Site

The AEP figure is obtained by combining the electrical power matrix with the probability distribution defined by the wave scatter diagram. Specifically:

$$AEP = (24 \times 365) \sum_{i=1}^{n} Pe(Hs_i, Te_i)\, p(Hs_i, Te_i) \qquad (5)$$

where Pe (Hs_i,Te_i) is the electrical power absorbed by the device for a given seastate defined by significant wave height Hs_i and wave energy period Te_i, and p (Hs_i,Te_i) is the probability of that seastate occurring at the site location. Assuming a rated power of 286kW, the official Sandia report on the RM3 device predicts an AEP figure of 700 MWh. The Flexcom software predicts an AEP value of 697.1 MWh, which is in excellent agreement with the published data on RM3. Figure 9 showed that the largest discrepancies between the linear and non-linear solution methodologies occurred for the larger seastates. The power capping tends to equalise all power values produced in larger waves, and so tends to compensate for any inaccuracies in the linear approach in the upper region. Because AEP is based on electrical rather than mechanical power, the overall energy production estimated by both solvers in very similar indeed.

VII. ECONOMICAL SCREENING TECHNIQUE

Numerical simulation of an entire scatter diagram in the time domain can be quite computationally expensive, so an economical extrapolation technique is proposed with a view to estimating the entire power production matrix based on a selection of 'reference seastates' within the scatter diagram. The scatter diagram is first sub-divided into 'blocks', where similar seastates are grouped together, before a single seastate is nominated as being representative for each block. Based on the numerical simulation results for the reference seastate within each block, a time history of power output is estimated for the remaining cells within the block, $P_{Cell}(t)$, using the following relationship.

$$P_{Cell}(t) = P_{Ref}(t) \frac{\int_0^\infty S_{Cell}(\omega) d\omega}{\int_0^\infty S_{Ref}(\omega) d\omega} \qquad (6)$$

where $P_{Ref}(t)$ is the time history of power output for the reference seastate, S_{Cell} is the wave elevation spectrum for the non-reference cell, and S_{Rref} is the wave elevation spectrum for the reference seastate. The average power output is then readily obtained from the extrapolated time history.

The mechanical power matrix presented in Figure 8 involved the dynamic analysis of 84 different seastates, each of which was simulated for 3600 seconds (1 hour) run-time, with an additional 100 seconds added for an initial ramp-up period which helps to dissipate initial transience in the numerical solution. Figure 12 presents a corresponding mechanical power matrix which is based on only 11 reference seastates (as highlighted by red markers in Figure 10 & Figure 12) which were explicitly simulated, with the remaining 73 cells estimated using the screening technique described above. For ease of comparison, Figure 13 presents the percentage error in mechanical power associated with the extrapolation process as a function of seastate. For this particular test case scenario:

- The maximum error in mechanical power for any given seastate is 12.6%.
- The average discrepancy across all seastates is just 1.8%.
- The potential savings in computational effort are over 80%.

Wave Height - Hs (m) \ Wave Period - Te (s)	4.5	5.5	6.5	7.5	8.5	9.5	10.5	11.5	12.5	13.5	14.5	15.5	16.5
0.25													
0.75		8	10	10	10	9	8	8	7	7	7	6	
1.25		24	27	29	27	25	22	22	20	19	19	18	
1.75		46	52	56	53	49	44	43	40	38	36	34	
2.25		76	86	93	87	82	72	71	65	62	60	57	
2.75		114	129	139	130	122	108	106	98	93	90	85	
3.25		159	180	193	182	170	151	149	137	130	125	119	
3.75		212	240	257	243	227	201	198	182	173	167	158	
4.25		272	308	331	312	292	259	254	233	222	214	203	
4.75		340	385	413	389	364	323	318	292	277	268	254	
5.25		416	470	505	475	445	395	388	356	339	327	310	
5.75		499	564	605	570	533	474	466	427	406	392	372	
6.25		590	666	715	674	630	560	550	505	480	463	440	
6.75													

Figure 12 : Mechanical Power Matrix for Eureka Site, estimated via screening approach

Hs (m) \ Te (s)	4.5	5.5	6.5	7.5	8.5	9.5	10.5	11.5	12.5	13.5	14.5	15.5	16.5
0.25													
0.75			0.0	0.0	0.0	0.0	0.0						
1.25		9.1	3.6	3.6	0.0	0.0	0.0	4.8	0.0				
1.75		0.0	0.0	0.0	0.0	2.0	0.0	2.4	0.0	0.0			
2.25		5.0	6.5	0.0	0.0	0.0	0.0	1.4	1.5	0.0			
2.75			10.4	0.0	1.5	0.0	0.0	0.0	0.0	0.0	2.3	1.2	
3.25			12.6	8.1	2.7	2.3	0.7	0.7	0.0	0.0	0.8		
3.75				7.2	7.3	3.0	3.4	0.0	0.0	0.0	0.6	0.0	
4.25						3.0	3.7	0.4	0.4	0.5	0.0	0.5	
4.75							9.0	0.6	0.3	0.4	0.0	0.4	
5.25							8.1	0.8	1.7	0.9	0.3		
5.75								0.4	3.0	1.0	0.5		
6.25								1.8	5.3	1.1			
6.75													

Figure 13 : Percentage Error in Mechanical Power associated with extrapolation process

Some caution is advised regarding the number and selection of reference seastates which are chosen to approximately represent the full scatter diagram. This process requires some engineering judgment, but conclusions reached from sensitivity studies led to the following simple guidelines:

- Generally speaking, any inaccuracies associated with the extrapolation process are likely to be more pronounced across different wave periods rather than wave heights. Hence, it is advisable to include at least one seastate block for each value of wave period in the scatter diagram.
- Responses at smaller wave amplitudes tend to be more linear than those at higher amplitudes, so smaller blocks should be used in regions of larger wave height.

VIII. EXPERIMENTAL TANK TESTS

A series of experimental tank tests was performed by NREL and Re Vision Consulting with a view to providing empirical data which could be helpful in validating numerical simulation studies [19]. Three sets of tank tests were performed in total at the University of California, and this study considers the third and most complex arrangement, which evaluates the power output from the device during operational wave conditions. Figure 14 shows the experimental setup, in which a 1/33 scale model of the device was connected to a set of four mooring lines. Each mooring line was connected to one of four metal piles located on the sidewall of the tank.

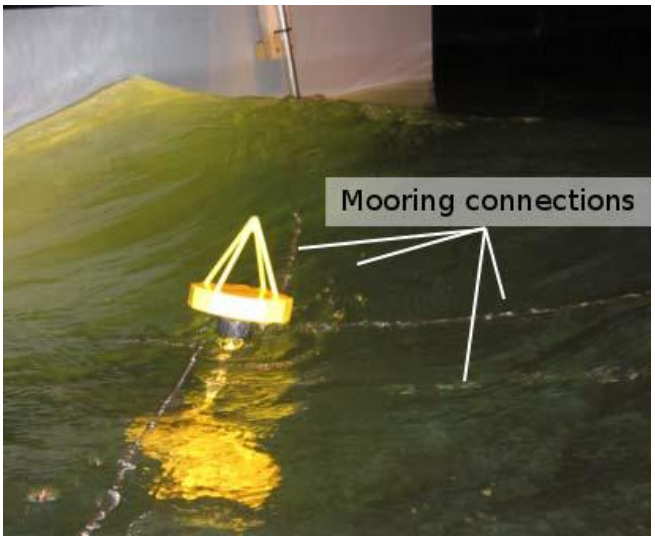

Figure 14 : Experimental Model [19]

A total of 33 test cases were performed during the experimental tank tests, of which 17 are considered in this report for ease of viewing (the experimental tests produced some duplicate data due to overlapping between similar test cases). Regular wave loading was simulated in the tank, with a target wave height of 3m (full scale) and a range of wave periods. The tests were performed for a range of PTO damping coefficients to maximize the design power output. Figure 15 and Figure 16 compare the experimental data to numerical simulations. For ease of inspection, the results are grouped into two sets of PTO ranges – Figure 15 considers PTO coefficients in the range of 2000 kNs/m to 2500 kNs/m, while Figure 16 presents results for PTOs of between 6100 kNs/m and 8100 kNs/m. Third-order polynomial regressions are included to represent the overall trends in power output.

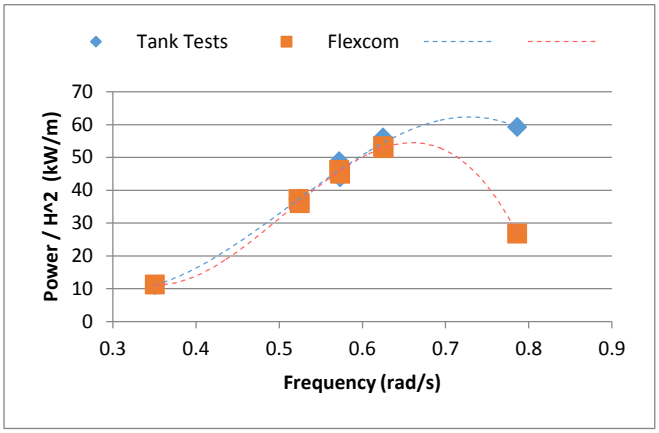

Figure 15 : Mechanical Power for Experimental Test Cases (PTO range: 2000 kNs/m – 2500 kNs/m)

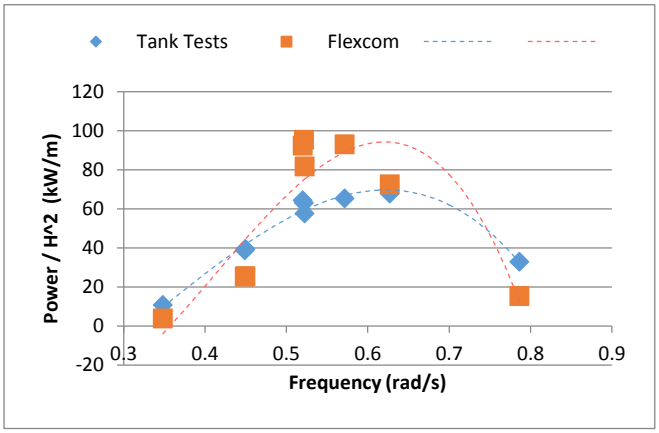

Figure 16 : Mechanical Power for Experimental Test Cases (PTO range: 6100 kNs/m – 8100 kNs/m)

Very close agreement of power output is demonstrated between experimental data and numerical simulations for the lower range of PTO damping coefficients. The overall trend is consistent, and of the 8 different wave frequencies considered, only one case (corresponding to the highest frequency / lowest period) shows any significant discrepancy. For the higher range of PTO coefficients, the results do not show a close correlation, with the numerical simulations appearing to overestimate power output from the device.

In mitigation, it should be noted that power output is directly influenced by PTO coefficient, and it has been acknowledged [19] that the research team had some difficulty in reproducing the desired PTO characteristics in the test tank. Despite two separate PTO models being attempted – firstly a miniature hydraulic cylinder in a closed hydraulic circuit, and secondly a hydraulic piston with multiple orifices – damping forces measured from the load cell were non-linear. For simplicity, the experimental team assumed that the relative motion is close to a harmonic function, and estimated an averaged PTO damping coefficient by the following relationship:

$$C_{PTO} = \frac{2P}{(\omega A_{rel})^2} \qquad (7)$$

where C_{PTO} is the estimated linear damping coefficient, P is the power output, A_{rel} is the relative motion between the float and the spar buoy, and ω is the incident wave frequency. In summary, the PTO settings in the experimental tests (non-linear) were not necessarily consistent with those used in the numerical simulations (linear). Note that it is possible to simulate non-linear damping characteristics in the software model, but sufficient information (i.e. time histories of instantaneous damping force from the experimental tests) was not available to pursue this avenue of research.

IX. CONCLUSION

Excellent agreement is obtained for regular wave simulations with 'WEC-Sim', an open-source simulation software widely used in the wave energy industry. For a real-world wave environment characterised by a full wave scatter diagram, good agreement is demonstrated with 'ANSYS Aqwa', a comprehensive modelling package which covers most fields of engineering simulation. Close agreement is also demonstrated with experimental tank test data, notwithstanding some uncertainty regarding non-linear PTO behaviour in the tank.

In summary, the modelling approach has proven capable of predicting device motions and power generation capabilities with high levels of confidence for low to medium wave periods, and crucially it represents a highly efficient computational solution technique. For more severe seastates, the theoretical assumptions underpinning a linear hydrodynamic modelling approach become increasingly invalid. In practice however the maximum power rating of the device imposed by generator sizes tends to compensate for any inaccuracies in the numerical solution.

The screening technique should prove very useful for preliminary feasibility studies, and also during sensitivity studies regarding design optimisation. As the design approaches finalisation, explicit simulation of all seastate combinations is strongly recommended as this will provide a more accurate estimate of operational performance. Additionally it will also allow the designer to quantify any inaccuracies associated with the screening approach.

In terms of future work, the numerical solver could be augmented via the inclusion of a more accurate hydrodynamic model (taking into consideration variations in the instantaneous wetted surface area). This would facilitate comparisons between the linear and non-linear models, and enable assessment of the overall significance of non-linear hydrodynamic effects.

ACKNOWLEDGMENT

The authors would like to compliment the U.S. Department of Energy on developing the reference model projects, and openly sharing information with the entire marine energy community. They would also like to thank Sandia National Laboratories for publishing the main technical report, and the NREL for sharing the experimental data.

REFERENCES

[1] National Renewable Energy Laboratory and Sandia Corporation (2015), WEC-Sim (Wave Energy Converter SIMulator). [Online at https://wec-sim.github.io/WEC-Sim/].

[2] Wood (2017), "Flexcom Theory Manual", Version 8.6. [Online at http://www.mcskenny.com/support/flexcom/theory.html].

[3] Ruehl, K., Michelen, C., Kanner, S., Lawson, M., & Yu, Y. H. (2014). "Preliminary verification and validation of WEC-Sim, an open-source wave energy converter design tool". In 33rd International Conference on Ocean, Offshore and Arctic Engineering, OMAE, San Francisco, CA, United States.

[4] Connolly, A. J., & Brewster, P. (2017, July). Application of Coupled Numerical Simulation to Design Wave Energy Converters. In The 27th International Ocean and Polar Engineering Conference. International Society of Offshore and Polar Engineers.

[5] O'Brien, P. J., Lane, M., & McNamara, J. F. (2002, January). "Improvements to the convected co-ordinates method for predicting large deflection extreme riser response". In ASME 2002 21st International Conference on Offshore Mechanics and Arctic Engineering (pp. 481-488). American Society of Mechanical Engineers.

[6] O'Brien, P. J., & McNamara, J. F. (1988, June). "Analysis of flexible riser systems subject to three-dimensional seastate loading". In Proceedings of the International Conference on Behavior of Offshore Structures (Vol. 3, pp. 1373-1388).

[7] Hall, M. (2015). MoorDyn—Users Guide. Department of Mechanical Engineering, University of Maine: Orono, ME, USA.

[8] Exceedence (2018), "Making Renewables Commercial". [Online at http://exceedence.com/]

[9] Sandia National Laboratories (2017), "Reference Model Project (RMP)". [Online at http://energy.sandia.gov/energy/renewable-energy/water-power/technology-development/reference-model-project-rmp/].

[10] Ocean Power Technologies (2017), "PB3 PowerBuoy". [Online at http://www.oceanpowertechnologies.com].

[11] Neary, V. S., Lawson, M., Previsic, M., Copping, A., Hallett, K. C., LaBonte, A., ... & Murray, D. (2014). "Methodology for design and economic analysis of marine energy conversion (MEC) technologies". SANDIA REPORT, SAND2014-9040. [Online at http://energy.sandia.gov/download/23111/].

[12] Cummins, W. E. (1962). The impulse response function and ship motions (No. DTMB-1661). David Taylor Model Basin Washington DC.

[13] Lee, C. H. (1995). WAMIT theory manual. Massachusetts Institute of Technology, Department of Ocean Engineering.

Morison, J. R., Johnson, J. W., & Schaaf, S. A. (1950). The force exerted by surface waves on piles. Journal of Petroleum Technology, 2(05), 149-154.

[14] Babarit, A., & Delhommeau, G. (2015, September). Theoretical and numerical aspects of the open source BEM solver NEMOH. In 11th European Wave and Tidal Energy Conference (EWTEC2015).

[15] Penalba Retes, M., Mérigaud, A., Gilloteaux, J. C., & Ringwood, J. (2015). "Nonlinear Froude-Krylov force modelling for two heaving wave energy point absorbers". In Proceedings of the 11th European Wave and Tidal Energy Conference. European Wave and Tidal Energy Conference 2015.

[16] Previsic, M., Shoele, K., & Epler, J. (2014). "Validation of theoretical performance results using wave tank testing of heaving point absorber wave energy conversion device working against a subsea reaction plate". In 2nd Marine Energy Technology Symposium (pp. 1-8).

[17] Yu, Y. H., & Li, Y. (2013). "Reynolds-Averaged Navier–Stokes simulation of the heave performance of a two-body floating-point absorber wave energy system". Computers & Fluids, 73, 104-114.

[18] Cargo, C. J., Plummer, A. R., Hillis, A. J., & Schlotter, M. (2012). Determination of optimal parameters for a hydraulic power take-off unit of a wave energy converter in regular waves. Proceedings of the Institution of Mechanical Engineers, Part A: Journal of Power and Energy, 226(1), 98-111.

[19] Yu, Y. H., Lawson, M., Li, Y., Previsic, M., Epler, J., & Lou, J. (2015). Experimental Wave Tank Test for Reference Model 3 Floating-Point Absorber Wave Energy Converter Project (No. NREL/TP--5000-62951). National Renewable Energy Lab.(NREL), Golden, CO (United States).

AUTHORS

First Author – Aengus Connolly, BE MEngSc MSc CEng, aengus.connolly@woodplc.com.

Second Author – Gerard O'Mahony, BE, gerard.omahony@woodplc.com.

Third Author – Aonghus O'Connor, BSc HDipAppSci PhD, aonghus.oconnor@woodplc.com.

Correspondence Author – Aengus Connolly, +353 (0)91 481 238.